Soft Matter

PAPER

Cite this: DOI: 10.1039/d1sm01798e

Experimental investigation of active noise on a rotor in an active granular bath

Ke Cheng,[a] Peng Liu,[abc] Mingcheng Yang*[abd] and Meiying Hou*[ab]

In an active bath, besides thermal noise, immersed passive objects also persistently experience collisions from active particles, which are often coarse-grained into a colored active noise with an assumed exponential time correlation. The exponentially correlated active noise extremely simplifies the theoretical description of immersed passive objects but so far lacks direct experimental verification. Here, we experimentally investigate the active noise subjected by a passive rotor confined in an active granular bath. On the basis of Langevin dynamics, we extract the characteristic of the active noise by analyzing the power spectrum of the rotor trajectory. Our experimental results find that the active noise experienced by the granular rotor does show an exponential time correlation to a good extent, even though due to the small experimental system and low collision frequency, the profile of the active noise in our system is non-Gaussian. Our findings give direct experimental evidence, which supports the widely-used active Ornstein–Uhlenbeck particle model in our dry active system.

Received 22nd December 2021,
Accepted 24th January 2022

DOI: 10.1039/d1sm01798e

rsc.li/soft-matter-journal

I. Introduction

Active matters, consisting of either natural[1,2] or synthetic[3–11] self-propelled units, can exhibit exotic non-equilibrium phenomena, since the active unit individually converts ambient energy into its motility. A large number of self-propelled particles constitute an active bath that significantly affects the structural and dynamical behaviors of immersed passive objects due to persistent collisions with the active particles. For example, in the active bath, the diffusion coefficient of the passive tracer can be orders of magnitude higher than that in the equilibrium thermal bath,[12] the non-symmetric objects can exhibit directional rotation,[13,14] and the efficiency of the Stirling-type heat engine will break through the Carnot limit.[15] Moreover, the active bath can give rise to unusual effective interactions between suspended passive objects[16] and unexpected self-assemblies.[17]

It is a formidable task to microscopically describe a passive object immersed in an active bath based on the inter-particle collisions, because of the many-body and out-of-equilibrium features. On the other hand, it has been long established that a passive Brownian particle in a thermal bath can be well described by the Langevin equation, which extremely simplifies the couplings of the particle and thermal bath as a damping force and a Gaussian white noise. Inspired by this well-known coarse-grained strategy, the interactions between the immersed passive object and abundant active particles have been simply treated as the frictional and active stochastic forces,[18] which could be reasonable on a large time scale. Nevertheless, in contrast to the white noise in the thermal bath, the active stochastic force is generally considered to be colored in order to capture the persistent collisions of the object with the self-propelling particles. Following the above scheme, a minimal theoretical description for the motion of passive objects in an active bath in the overdamped limit reads,

$$\gamma\frac{\mathrm{d}}{\mathrm{d}t}\vec{r}(t) = -\nabla U(\vec{r}) + \vec{f}(t), \tag{1}$$

where γ refers to the damping coefficient and $U(\vec{r})$ to the external potential. For convenience, the active stochastic force $\vec{f}(t)$ is usually assumed as an exponentially correlated noise with zero mean and variance,

$$\langle f_i(t) f_j(t') \rangle = \delta_{ij}\frac{D_\mathrm{A}}{\tau}\exp\left(-\frac{|t-t'|}{\tau}\right), \tag{2}$$

with D_A and τ being the strength and correlation time of the active noise, respectively.

This minimal model has not only been extensively used to investigate the dynamics of passive objects in an active bath,[12,19–22] but also been applied to mimic the active particles themselves,[23] namely the so-called Active Ornstein–Uhlenbeck particles (AOUP). Particularly, eqn (1) and (2) provide an ideal starting point to study the stochastic thermodynamics of active systems.[24–27] Although the assumption of the exponentially

[a] Beijing National Laboratory for Condensed Matter Physics and Laboratory of Soft Matter Physics, Institute of Physics, Chinese Academy of Sciences, Beijing 100190, China. E-mail: mcyang@iphy.ac.cn, mayhou@iphy.ac.cn
[b] School of Physical Sciences, University of Chinese Academy of Sciences, Beijing 100049, China
[c] Wenzhou Institute, University of Chinese Academy of Sciences, Wenzhou, Zhejiang 325001, China
[d] Songshan Lake Materials Laboratory, Dongguan, Guangdong, 523808, China

correlated active noise allows analytical treatment and successfully reproduces many essential properties of active systems, its direct experimental evidence is still lacking.

In order to investigate the characteristics of active noise, in this paper a passive rotor suspended in an active granular bath is used. A passive rotor has been used previously for passive granular systems to study the ratchet effects[28] and fluctuation relations.[29,30] The rotor has only one degree of freedom and its motion can be determined by collisions with the particles. We therefore extend the use of the rotor as a probe to explore the noise in an active bath.

Here, the active bath is composed of asymmetric particles excited by a vertically vibrating shaker. In experiments, we record the angular trajectory of the passive rotor and apply a spectral analysis method[31] to extract the parameters of active noise in the framework of the Langevin equation. Compared with the determination of the mean square displacement of the passive tracer in an active bath,[12,20] the spectral analysis method provides direct evidence of the existence of the colored active noise. Our results clearly indicate that the active noise experienced by the passive rotor in the active granular bath is indeed correlated exponentially to a good extent, strongly supporting the widely-used theoretical assumption on the active noise.

The rest of the paper is organized as follows: Section II gives detailed information on the experimental setup. Section III (A) shows an experiment result of an equilibrium-like granular bath to verify the accuracy and reliability of the spectrum analyzing method. Section III (B) applies this method to the active system. Section III (C) discusses the memory effect in the active granular bath. Section IV presents a brief conclusion.

II. Experimental setup

We implement experiments to examine the AOUP model for a passive rotor immersed in an active granular fluid by using an apparatus improved on the basis of our previous work,[32] as sketched in Fig. 1. The passive rotor is made of nylon and is connected to a shaft (the blue part in Fig. 1(a) and (b)) with a ceramic bearing to minimize the static friction. The bearing is embedded into a transparent top cover. The container with a height of 2.5 cm and inner diameter of 19 cm is fixed on a vertically vibrating table (V.T.). A spiral spring is at the top cover, whose two ends are separately linked to the shaft and the cover. To avoid the interference of the electrostatic interaction between particles and collisions against container walls, we sprayed antistatic fluid to the inside walls of the container and the particle surface. The granular gas is composed of plastic polyhedrons for the passive bath [Fig. 1(d)] and eccentric cylindric tubes for the active bath [Fig. 1(c)]. Owing to the collisions with granular particles, the rotor exhibits a random rotation, whose trajectory is recorded by a high-speed camera (QHYCCD 174M). To precisely track the angular position of the rotor $\theta(t)$, a black dot with a diameter of 0.5 cm is marked on the rotor paddle. The tracking uncertainty (0.002 rad) caused by

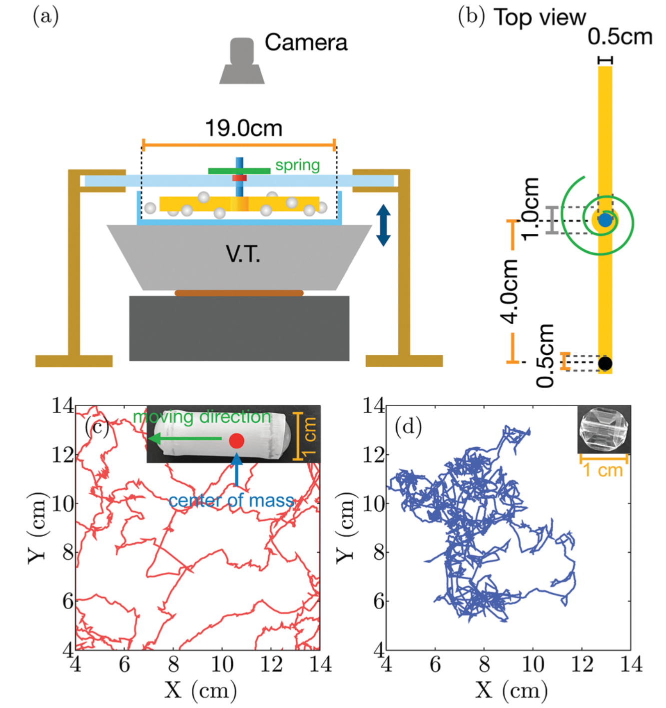

Fig. 1 (a) The experimental apparatus. V. T. is the vibration table. (b) Top view of the rotor and spiral spring. The trajectory of a single (c) active and (d) passive particle in experiments. Both trajectories are obtained during a time interval of 30 seconds.

the camera noise is experimentally checked by tracking the $\theta(t)$ when there is no particle in the container. The uncertainty is small enough and can be neglected.

From the angular position of the passive rotor, its angular velocity can be determined by $\omega(t) \simeq (\Delta\theta)/t_f$, with t_f the time interval between two consecutive frames. The frame rate of the camera is chosen to be 200 fps in the experiment. Both of the passive and active experiments are repeated four times.

III. Results and discussion

A. Passive bath

The passive bath consists of 103 plastic polyhedrons in the container. Each polyhedral particle has a mass of 0.52 grams and diameter of 1.0 cm on average. The packing fraction of particles is ϕ = 0.36 and the mean free path is around 2.48 cm. In the experiment, the vibration frequency is fixed at 50 Hz and the vibration acceleration is 3.0g. Our experimental data contains 3×10^5 frames (the corresponding experimental duration is 25 minutes).

The motion of the rotor confined by a spring follows the Langevin equation:

$$\ddot{\theta} + \Gamma\dot{\theta} + \partial_\theta V(\theta)/I = \xi(t), \tag{3}$$

where I is the moment of inertia, Γ is the scaled damping coefficient resulting from collisions with the contained particles, and $V(\theta) = \frac{1}{2}k\theta^2$ is the external harmonic potential contributed by the spring. $\xi(t)$ is assumed to be a white noise, which is described by a delta-correlation, $\langle\xi(t)\xi(t')\rangle = 2D\delta(t-t')$, where D is the noise strength. We introduce a scaled stiffness $K = k/I$.

Fig. 2(a) shows the distribution of the angular velocity $P_1(\omega)$, which can be well fitted by a Gaussian function with the variance $\langle\omega^2\rangle = 0.26\ \mathrm{rad}^2\ \mathrm{s}^{-2}$. This indicates that the rotor in the passive bath is in an equilibrium-like state. We therefore employ the equilibrium statistics to determine the stiffness K of the potential $V(\theta)$, and verify the accuracy and reliability of the spectral analysis method, which will be used to extract the active noise later.

Utilizing the fact that the degrees of freedom of the rotor obey the Boltzmann distribution, the joint distribution function of θ and ω thus reads

$$P(\theta,\omega) \propto \exp\left[-\left(\frac{1}{2}I\omega^2 + V(\theta)\right)/k_{\mathrm{B}}T\right], \quad (4)$$

with T the effective temperature which is related to the fluctuation of the angular velocity *via* the equipartition theorem $k_{\mathrm{B}}T = I\langle\omega^2\rangle$. Integrating over ω yields the probability distribution of θ,

$$P_2(\theta) = \frac{1}{Z}\exp\left[-\frac{V(\theta)}{k_B T}\right], \quad (5)$$

where Z is the normalization factor. Hence, the external potential $V(\theta)$ can be directly obtained from the experimentally measured $P_2(\theta)$,

$$V(\theta) = -k_B T\ln P_2(\theta) - k_B T\ln Z, \quad (6)$$

as shown in Fig. 2(b). The obtained external potential can be well fitted by a quadratic function, which yields the scaled stiffness coefficient $K = 101 \pm 0.8\ \mathrm{s}^{-2}$. The K value can also be verified by directly using the equipartition theorem, in which the mean kinetic and potential energy of the rotor are equal, $\langle\omega^2\rangle = K\langle\theta^2\rangle$. This gives us a value $K = 103 \pm 0.9\ \mathrm{s}^{-2}$, which is consistent with the previous K value of $101\ \mathrm{s}^{-2}$.

We now apply the power spectrum density (PSD) method to solve the parameters Γ and K of the motion of the passive rotor. Here, the stochastic dynamics can be transformed to Fourier space:

$$\tilde{\theta}(\nu) = \int_{-\infty}^{\infty}\theta(t)\exp(-i\nu t)\mathrm{d}t, \quad (7)$$

and the PSD of $\omega(t)$ is

$$S_\omega(\nu) = \lim_{T\to\infty}\frac{1}{T}|\tilde{\omega}(\nu)|^2\ldots = \int_{-\infty}^{\infty}\left[\lim_{T\to\infty}\frac{1}{T}\int_{-T/2}^{T/2}\omega(t)\omega(t+\tau)\mathrm{d}t\right]e^{-i\nu\tau}\mathrm{d}\tau \quad (8)$$

Eqn (3) in Fourier space is written as

$$-\nu^2\tilde{\theta}(\nu) + i\nu\Gamma\tilde{\theta}(\nu) + K\tilde{\theta}(\nu) = \tilde{\xi}(\nu). \quad (9)$$

After some algebra, we obtain the expression of the power spectrum

$$S_\omega(\nu) = \frac{2D\varepsilon\nu^2}{(\nu^2-K)^2 + \Gamma^2\nu^2}, \quad (10)$$

where ε is a normalization factor. Therefore, by fitting eqn (10) to the measured PSD data, we can determine the parameters Γ and K.

Fig. 3(a) plots the power spectrum density *versus* angular frequency $\nu/2\pi$. The maximum frequency is taken as 100 Hz, which is half of the frame rate. For the sake of preciseness, a moving-window average of 10 points is added to Fig. 3. The Levenberg–Marquardt algorithm is used to fit the spectrum curves (blue curve in Fig. 3). We obtained $\Gamma = 11.3 \pm 0.1\ \mathrm{s}^{-1}$ and $K = 101 \pm 0.5\ \mathrm{s}^{-2}$ from the fitted curve in Fig. 3(a). The obtained K value is consistent with the value obtained from the Boltzmann distribution. This indicates that the spectral analysis method is reliable to extract the system dynamical parameters.

Inserting the known Γ, K and the measured $\theta(t)$ into the Langevin eqn (3), $\xi(t) = \ddot{\theta} + \Gamma\dot{\theta} + K\theta$, the power spectrum of the noise can be calculated. As shown in Fig. 3(b), the noise ξ in

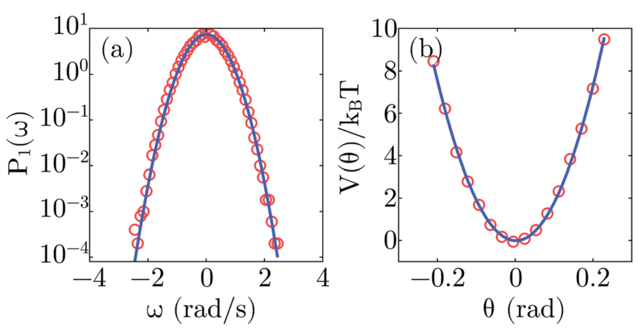

Fig. 2 (a) The distribution of angular velocity which is fitted with a Gaussian function (the blue curve). (b) The spring potential determined by eqn (6) based on the experimentally measured $P_2(\theta)$. The blue curve refers to a quadratic fitting.

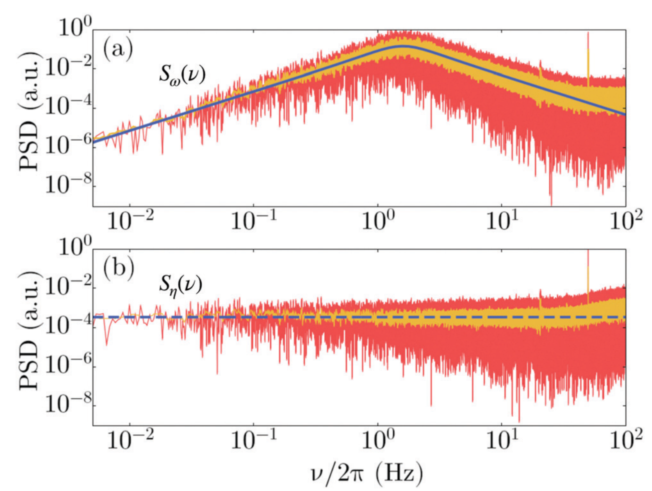

Fig. 3 (a) The power spectrum density of the angular velocity ω. The red curve is the original data, and the yellow curve denotes the smoothed data. The blue curve corresponds to the result obtained by fitting with eqn (10). (b) The power spectrum of the noise extracted through $\ddot{\theta} + \Gamma\dot{\theta} + K\theta$.

the passive system is a good white noise. In the following, we apply the spectra analysis method to the active bath to extract the characteristics of the active noise.

B. Active bath

The active particle is made of a plastic tube with 1 cm diameter and 3 cm length, as shown in Fig. 1(c). This type of rod-like particle has been extensively used as an active particle in previous studies.[8,33,34] To break the symmetry of the tube, two 1 cm-diameter beads of materials with different densities (here glass and plastics beads are used) are separately embedded into the two ends of the tube. As a result, the tube self-propels along its long axis on the vibrating substrate. In the experiment, the vibration acceleration of the vibrating table is $4.0g$, and the vibration frequency is 50 Hz. We choose a moderate packing fraction, $\phi = 0.39$. This is because too high a packing fraction can give rise to self-assembly behaviors (clustering), and too low a packing fraction will keep the rotor free of any collision for most of the time.

The present rotor is symmetrical so that it fluctuates around the equilibrium position of the externally confined potential. Unlike the ratchet system,[35] the rotor does not apply directional torque to the active bath. Although the rotation angle fluctuates randomly, its angular velocity distribution deviates from the Gaussian function (see Fig. 4), and the equipartition theorem does not apply. The definition of temperature is not involved in the active bath. The out-of-equilibrium feature of the rotor does not, however, influence the use of spectral analysis in the active noise.

We assume that the passive rotor in the active bath can still be described by the underdamped Langevin equation,[36]

$$\ddot{\theta}(t) + \Gamma_0\dot{\theta}(t) + K'\theta(t) = \eta(t) + \xi_1(t), \tag{11}$$

with Γ_0 is the damping coefficient and K' is the effective stiffness of the external spring, which are regarded as free parameters. For simplicity, the frictional term is considered memory-less (without a memory kernel).

Here, besides the white thermal noise $\xi_1(t)$ with the variance $\langle\xi_1(t)\xi_1(t')\rangle = 2B_{\mathrm{T}}\delta(t-t')$, an independent colored active noise $\eta(t)$ is included to capture the persistent collisions of the rotor with the active particles. As extensively used in the literature,[12,19–22] $\eta(t)$ is assumed to be exponentially correlated $\langle\eta(t)\eta(t')\rangle = B_{\mathrm{A}}/\Gamma_{\mathrm{a}}\exp(-\Gamma_{\mathrm{a}}|t-t'|)$, namely it obeys the Ornstein-Uhlenbeck process:[23,37]

$$\dot{\eta}(t) + \Gamma_{\mathrm{a}}\eta(t) = \xi_2(t). \tag{12}$$

where $\langle\xi_2(t)\xi_2(t')\rangle = 2B_{\mathrm{A}}\delta(t-t')$. The Fourier transform of eqn (11) and (12) yields:

$$-\nu^2\tilde{\theta}(\nu) + i\nu\Gamma_0\tilde{\theta}(\nu) + K'\tilde{\theta}(\nu) = \tilde{\eta}(\nu) + \tilde{\xi}_1(\nu) \tag{13}$$

$$i\nu\tilde{\eta}(\nu) + \Gamma_{\mathrm{a}}\tilde{\eta}(\nu) = \tilde{\xi}_2(\nu) \tag{14}$$

Substituting eqn (14) into eqn (13), the power spectra of the angular velocity $\omega(t)$ becomes

$$S_\omega(\nu) = \frac{\nu^2}{(\nu^2 - K')^2 + \Gamma_0^2\nu^2}\left(\frac{2B_{\mathrm{A}}\varepsilon}{\Gamma_{\mathrm{a}}^2 + \nu^2} + 2B_{\mathrm{T}}\varepsilon\right). \tag{15}$$

And, the power spectra of total noise $S_N(\nu)$ and active noise $S_\eta(\nu)$ separately read

$$S_N(\nu) = 2B_{\mathrm{A}}\varepsilon/(\Gamma_{\mathrm{a}}^2 + \nu^2) + 2B_{\mathrm{T}}\varepsilon \tag{16}$$

and

$$S_\eta(\nu) = 2B_{\mathrm{A}}\varepsilon/(\Gamma_{\mathrm{a}}^2 + \nu^2). \tag{17}$$

The parameters (Γ_0, Γ_{a}, K', B_{T}, B_{A}) can be determined by fitting eqn (15) to the power spectrum obtained from experiments. In order to ensure that the fitting result is reasonable and unique, we determine the independent parameters in a stepwise manner [see Appendix (A)]. The experimental data of the power spectrum of ω can be well fitted by eqn (15), as plotted in Fig. 5(a), in which the blue curve is the fitted result

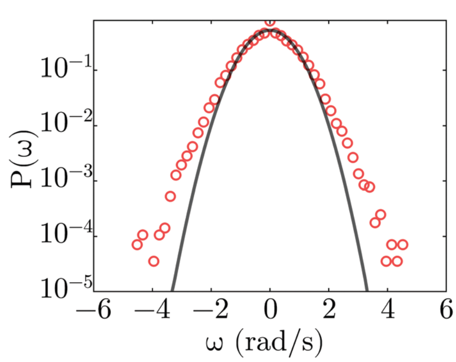

Fig. 4 The angular velocity distribution of the rotor in the active bath. The black curve is a Gaussian fitting.

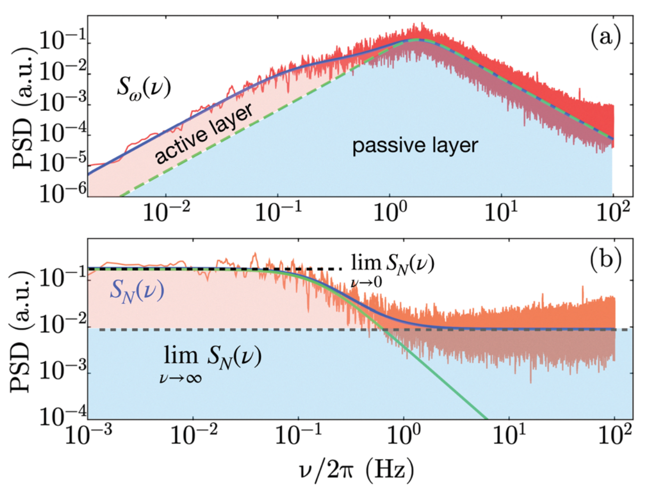

Fig. 5 (a) The power spectrum density of ω. The red curve is the smoothed data after a 10 − point moving-window average, and the blue curve is the fitting result using eqn (15). For reference, the equilibrium counterpart is also plotted by taking $B_{\mathrm{A}} = 0$ in eqn (15) (the dashed green curve). (b) The power spectrum of total noise $N_{\mathrm{tot}} = \xi_1 + \eta$, where the red and blue curves correspond to the experimental data and theoretical fit with eqn (16), respectively. For comparison, the power spectrum of the pure active noise $S_\eta(\nu)$ given by eqn (17) is plotted (the green curve).

with parameters $\Gamma_0 = 15.8 \pm 0.06\ \mathrm{s}^{-1}$, $\Gamma_a = 0.94 \pm 0.08\ \mathrm{s}^{-1}$, $K' = 130 \pm 1.5\ \mathrm{s}^{-2}$, $B_A\varepsilon = 235 \pm 14\ \mathrm{s}^{-5}$, and $B_T\varepsilon = 14.4 \pm 0.11\ \mathrm{s}^{-3}$. The ratio of B_A to B_T measures the intensity of the active noise relative to the thermal noise.

Eqn (15) and Fig. 5(a) indicate that the power spectrum is a superposition of the passive and active parts. For comparison, we plot the referenced spectrum curve with $B_A = 0$ (the green dashed curve in Fig. 5(a)). It is clear that the power spectrum of ω consists of two distinct layers, in which the blue region corresponds to $\ddot{\theta}(t) + \Gamma_0\dot{\theta}(t) + K'\theta(t) = \xi_1(t)$, contributed by the thermal noise, and the red region represents the contribution from the active noise.

To extract the power spectrum of the noise, the obtained parameters $K' = 130\ \mathrm{s}^{-2}$ and $\Gamma_0 = 15.8\ \mathrm{s}^{-1}$ are substituted into eqn (11), such that the total noise reads $N_{\mathrm{tot}}(t) = \ddot{\theta}(t) + \Gamma_0\dot{\theta}(t) + K'\theta(t) = \xi_1(t) + \eta(t)$. The orange curve in Fig. 5(b) shows the smoothed power spectrum density of N_{tot}. This power spectrum of the noise can still be separated into two superposed parts. The power spectrum of N_{tot} at $\nu \to 0$ is dominated by the active noise η and can be well described by eqn (17); while at $\nu \to \infty$ the white noise ξ_1 is dominant and the active noise is negligible. So, the self-propulsion mainly affects the low-frequency band. The good agreement between eqn (17) and the low-frequency spectrum thus provides direct evidence that the passive rotor in the active granular bath is subjected to an exponentially-correlated active noise.

Fig. 6 plots the autocorrelation function $C(t - t') = \langle N_{\mathrm{tot}}(t)N_{\mathrm{tot}}(t')\rangle$, which shows an exponential decay against the time difference with a delta-correlation for $t = t'$. This dependence can be understood in terms of the following simple calculation,

$$\begin{aligned}\langle N_{tot}(t)N_{tot}(t')\rangle = \langle\xi_1(t)\xi_1(t')\rangle + 2\langle\xi_1(t)\eta(t')\rangle \\ + \langle\eta(t)\eta(t')\rangle.\end{aligned} \quad (18)$$

Here, the first term corresponds to the white noise, which obeys the Dirac-delta function $\langle\xi_1(t)\xi_1(t')\rangle = 2B_T\delta(t - t')$; the second term vanishes because of the independence of the two noises,

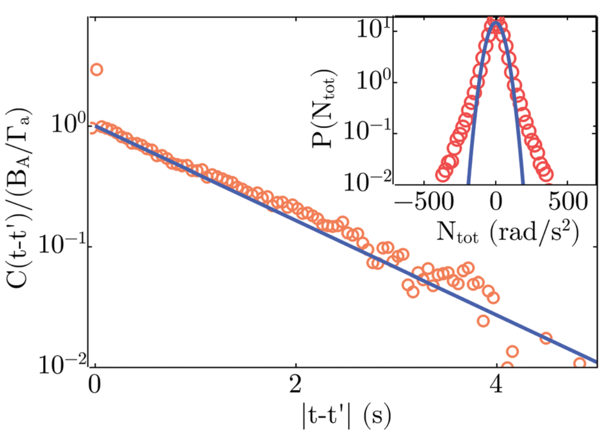

Fig. 6 The normalized correlation function of the total noise. Here, the blue line corresponds to the exponential function $C(t - t')/(B_A/\Gamma_a) = \exp(-\Gamma_a|t - t'|)$, calculated from eqn (18). The inset plots the distribution of N_{tot}, with the blue curve being a Gaussian fit.

and the third term (active noise) is expected to be exponentially decayed $\langle\eta(t)\eta(t')\rangle = B_A/\Gamma_a \exp(-\Gamma_a|t - t'|)$. Eqn (18) quantitatively agrees with the auto-correlation data obtained from the experiment, which again supports that the rotor dynamics in the active granular bath can be described by the AOUP model.

The inset of Fig. 6 displays the distribution of N_{tot} that deviates from the Gaussian distribution, since in the present small experimental system the collision times are insufficient to ensure the central limit theorem. Nevertheless, the non-Gaussian property of the noise does not prevent us from studying its time correlation. The result indicates that the AOUP model can be applied to small systems even with a non-Gaussian active noise.

Finally, it should be noted that the effective stiffness of the spiral spring $K' = 130\ \mathrm{s}^{-2}$ extracted from the active bath deviates from $K = 101\ \mathrm{s}^{-2}$ determined in the equilibrium-like situation. However, the stiffness coefficient of the external spring should be independent of the type of the granular particles. We speculate that the deviation could arise from the frictional memory effect that may exist in the present active granular system but is ignorable in bacterial solutions.[38] In the following section, we show that the difference in the stiffness coefficient can be reasonably explained using the Langevin equation with a frictional memory kernel.

C. Memory effect in active granular gas

In general, the friction acting on the particle in the Langevin equation can depend on the history of the system, which is referred to as the memory effect. For a confined particle in the equilibrium solvent, the memory effect on the picosecond scale is confirmed by computer simulation.[39] In macroscopic systems, the memory effect may be observed on longer time scales. It has been reported that the memory effect occurs in crowded granular systems,[40] and the direct cause of the memory effect is the repeated collisions. In our experiment, with a moderate packing fraction, the recollisions between the active particles and the rotor are caused by the persistent self-propulsion of the active particles, and the self-propulsion originates from the asymmetry of the particle.

In the following, we assume that the passive rotor in the active granular bath is also affected by the memory, and demonstrate that the effective stiffness K' in eqn (11), which deviates from the stiffness K determined in the passive bath, could be caused by the frictional memory effect in the active bath.

Replacing the friction with a kernel convolution, eqn (11) becomes the generalized Langevin equation (GLE):

$$\ddot{\theta}(t) + \int_{-\infty}^{\infty} \Gamma(t - t')\dot{\theta}(t')\mathrm{d}t' + K\theta(t) = \eta(t) + \xi_1(t). \quad (19)$$

It is physically required that $\Gamma(t)$ satisfies the causality, thus $\Gamma(t)$ should be zero at $t < 0$. On the other hand, the memory effect will vanish for a sufficiently long time, *i.e.*,

$$\lim_{t\to\infty} \Gamma(t) = 0.$$

Although the memory kernel is difficult to measure directly from the experiment, we can make a reasonable assumption. In

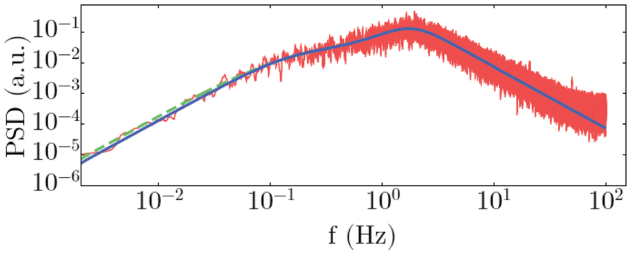

Fig. 7 The power spectrum fitted with eqn (15) obtained from the normal Langevin equation (solid blue curve), and with eqn (22) based on the GLE (dashed green curve). The fitting parameters obtained from eqn (22) are $B_A\varepsilon = 237 \pm 15\ s^{-5}$, $B_T\varepsilon = 14.39 \pm 1.2\ s^{-3}$, $c_1 = 29.1 \pm 4.9\ s^{-2}$, $c_2 = 15.7 \pm 0.35\ s^{-1}$, $\alpha = 0.467 \pm 0.16\ s^{-1}$ and $\Gamma_a = 1.03 \pm 0.5\ s^{-1}$, where $K = 101\ s^{-2}$ remains fixed.

terms of the above requirements, we assume the memory kernel is the combination of a Dirac-delta function and an exponential decay function:

$$\Gamma(t) = c_1 e^{-\alpha t}\Theta(t) + c_2\delta(t). \tag{20}$$

Θ is the Heaviside step function and $1/\alpha$ (>0) represents the characteristic memory time. Substituting eqn (20) into eqn (19) and taking a Fourier transform, we have

$$\begin{aligned} S_\omega(\nu) &= \frac{\nu^2}{|-\nu^2 + K + i\nu\Gamma(\nu)|^2}\left(\frac{2B_A\varepsilon}{\Gamma_a^2+\nu^2} + 2B_T\varepsilon\right), \\ \Gamma(\nu) &= \frac{c_1}{\alpha + i\nu} + c_2. \end{aligned} \tag{21}$$

After some algebra, the power spectrum of ω is

$$\begin{aligned} S_\omega(\nu) &= \left(\frac{2B_A\varepsilon}{\Gamma_a^2+\nu^2} + 2B_T\varepsilon\right)\frac{\nu^2}{P}, \\ P &= (\nu^2 - K)^2 + \frac{\nu^2}{\alpha^2+\nu^2}(c_1^2 + 2c_1c_2\alpha) \\ &\quad - \frac{\nu^2(\nu^2-K)2c_1}{\alpha^2+\nu^2} + c_2^2\nu^2 \end{aligned} \tag{22}$$

We employ eqn (22) to fit the power spectrum of the angular velocity. Fig. 7(a) shows that eqn (22) can indeed well fit the power spectrum, where the stiffness coefficient of the external spring $K = 101\ s^{-2}$, determined from the passive system, remains fixed. This result thus supports our argument that the difference between the stiffness coefficient K' (obtained from the active bath) and K (the passive bath) may originate from the friction memory kernel.

IV. Conclusions

The Langevin equation with a colored active noise, which captures the persistent collisions of active particles on a coarse-grained time scale, provides an ideal scheme to study the non-equilibrium behavior of objects immersed in active baths. In this scheme, a critical assumption is that the colored active noise is considered to be exponentially correlated in time. Here, we experimentally investigate the properties of the active noise experienced by a harmonically confined passive rotor in an active granular bath. By means of spectral analysis justified in a passive granular bath, we extract all the parameters of the Langevin equation governing the dynamics of the passive rotor in the active bath. The results indicate that the active noise suffered by the rotor is indeed exponentially correlated to a good extent. Our work supports the frequently used hypothesis of exponentially correlated active noise, thus giving direct experimental evidence that the passive object in the active bath can be described by the AOUP model. Furthermore, our work suggests that the spectral analysis provides a powerful tool for studying the kinetic parameters of other dry passive systems, like the vibrating isotropic disk,[41] and wet active systems, such as colloidal particles suspended in a bacterial solution.[2]

Conflicts of interest

There are no conflicts to declare.

Appendix A: details for fitting the power spectrum

Eqn (15) contains five independent parameters, and fitting all five variables at once will lead to unreasonable results. In this experiment, we adopt a stepwise fitting method to ensure the reasonableness and uniqueness of the results. The workflow of fitting is shown in Fig. 8(b).

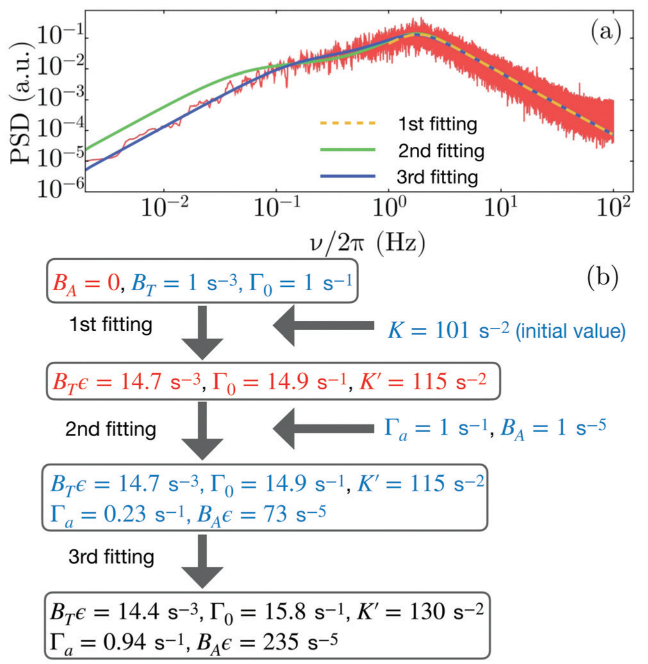

Fig. 8 Fitting procedure. (a) The yellow, green and blue curves correspond to the first, second and third fittings, respectively. (b) The flow chart of the fitting. Red numbers are constant terms for the next fitting procedure, and blue numbers denote initial values. The frequency range for the first fitting is 1–100 Hz, and the other two fittings are implemented in a range of 0.001–100 Hz.

As $\nu \to \infty$, the component $2B_A\varepsilon/(\Gamma_a{}^2 + \nu^2)$ in eqn (15) vanishes, and the $S_\omega(\nu)$ reduces to the equilibrium case. This means that the self-propulsion will hardly affect the high-frequency band. In the first fitting procedure, we utilize the high-frequency part (1–100 Hz) to estimate Γ_0, K', and $B_T\varepsilon$, which yields the yellow dashed curve in Fig. 8(a).

In the second fitting procedure, we introduce the other two parameters $B_A\varepsilon$ and Γ_a, which are related to the active noise $\eta(t)$ in the dynamics [see eqn (17)]. As shown in Fig. 8(b), the three parameters associated with the thermal noise remain constant. The result of the second fitting step is plotted as the green curve in Fig. 8(a).

The above two fitting procedures roughly determine the five independent parameters. In order to achieve an accurate fitting result, we performed the third fitting step on the basis of these obtained parameters, which is represented by the blue curve in Fig. 8(a), in good agreement with the power spectrum.

Acknowledgements

We greatly acknowledge the support of the National Natural Science Foundation of China (No. 11874397 and U1738120), the Strategic Priority Research Program of Chinese Academy of Sciences (No. XDB33000000), the ESA—CMSA/CSU Space Science and Utilization collaboration program, and YYWT-0601-EXP-20.

References

1 P. J. A. Janssen and M. D. Graham, Coexistence of tight and loose bundled states in a model of bacterial flagellar dynamics, *Phys. Rev. E: Stat., Nonlinear, Soft Matter Phys.*, 2011, **84**, 011910.

2 R. Di Leonardo, L. Angelani, D. Dell'Arciprete, G. Ruocco, V. Iebba and S. Schippa, *et al.*, Bacterial ratchet motors, *Proc. Natl. Acad. Sci. U. S. A.*, 2010, **107**(21), 9541–9545.

3 H. R. Jiang, N. Yoshinaga and M. Sano, Active Motion of a Janus Particle by Self-Thermophoresis in a Defocused Laser Beam, *Phys. Rev. Lett.*, 2010, **105**, 268302.

4 J. Palacci, S. Sacanna, A. P. Steinberg, D. J. Pine and P. M. Chaikin, Living crystals of light-activated colloidal surfers, *Science*, 2013, **339**(6122), 936–940.

5 W. F. Paxton, K. C. Kistler, C. C. Olmeda, A. Sen, S. K. Angelo and Y. Cao, *et al.*, Catalytic nanomotors: autonomous movement of striped nanorods, *J. Am. Chem. Soc.*, 2004, **126**(41), 13424–13431.

6 I. Theurkauff, C. Cottin-Bizonne, J. Palacci, C. Ybert and L. Bocquet, Dynamic clustering in active colloidal suspensions with chemical signaling, *Phys. Rev. Lett.*, 2012, **108**(26), 268303.

7 I. Buttinoni, J. Bialké, F. Kümmel, H. Löwen, C. Bechinger and T. Speck, Dynamical clustering and phase separation in suspensions of self-propelled colloidal particles, *Phys. Rev. Lett.*, 2013, **110**(23), 238301.

8 L. J. Daniels, Y. Park, T. C. Lubensky and D. J. Durian, Dynamics of gas-fluidized granular rods, *Phys. Rev. E: Stat., Nonlinear, Soft Matter Phys.*, 2009, **79**, 041301.

9 L. Walsh, C. G. Wagner, S. Schlossberg, C. Olson, A. Baskaran and N. Menon, Noise and diffusion of a vibrated self-propelled granular particle, *Soft Matter*, 2017, **13**(47), 8964–8968.

10 P. Liu, H. Zhu, Y. Zeng, G. Du, L. Ning and D. Wang, *et al.*, Oscillating collective motion of active rotors in confinement, *Proc. Natl. Acad. Sci. U. S. A.*, 2020, **117**(22), 11901–11907.

11 C. Scholz and T. Pöschel, Velocity Distribution of a Homogeneously Driven Two-Dimensional Granular Gas, *Phys. Rev. Lett.*, 2017, **118**, 198003.

12 C. Maggi, M. Paoluzzi, N. Pellicciotta, A. Lepore, L. Angelani and R. Di Leonardo, Generalized Energy Equipartition in Harmonic Oscillators Driven by Active Baths, *Phys. Rev. Lett.*, 2014, **113**, 238303.

13 M. J. Y. Jerez, M. A. Bonachita and M. N. P. Confesor, Dynamics of a ratchet gear powered by an active granular bath, *Phys. Rev. E*, 2020, **101**, 022604.

14 H. Li, X. Yang and H. Zhang, Symmetry properties of fluctuations in an actively driven rotor, *Chin. Phys. B*, 2020, **29**(6), 060502.

15 S. Krishnamurthy, S. Ghosh, D. Chatterji, R. Ganapathy and A. Sood, A micrometre-sized heat engine operating between bacterial reservoirs, *Nat. Phys.*, 2016, **12**(12), 1134–1138.

16 P. Liu, S. Ye, F. Ye, K. Chen and M. Yang, Constraint dependence of active depletion forces on passive particles, *Phys. Rev. Lett.*, 2020, **124**(15), 158001.

17 Z. Shen, A. Würger and J. S. Lintuvuori, Hydrodynamic selfassembly of active colloids: chiral spinners and dynamic crystals, *Soft Matter*, 2019, **15**(7), 1508–1521.

18 X. L. Wu and A. Libchaber, Particle Diffusion in a Quasi-Two-Dimensional Bacterial Bath, *Phys. Rev. Lett.*, 2000, **84**, 3017–3020.

19 S. Das, G. Gompper and R. G. Winkler, Confined active Brownian particles: theoretical description of propulsion-induced accumulation, *New J. Phys.*, 2018, **20**(1), 015001.

20 S. Ye, P. Liu, F. Ye, K. Chen and M. Yang, Active noise experienced by a passive particle trapped in an active bath, *Soft Matter*, 2020, **16**, 4655–4660.

21 A. Argun, A. R. Moradi, E. Pinçe, G. B. Bagci, A. Imparato and G. Volpe, Non-Boltzmann stationary distributions and nonequilibrium relations in active baths, *Phys. Rev. E*, 2016, **94**, 062150.

22 S. Chaki and R. Chakrabarti, Entropy production and work fluctuation relations for a single particle in active bath, *Phys. A*, 2018, **511**, 302–315.

23 Y. Fily and M. C. Marchetti, Athermal Phase Separation of Self-Propelled Particles with No Alignment, *Phys. Rev. Lett.*, 2012, **108**, 235702.

24 L. Dabelow, S. Bo and R. Eichhorn, Irreversibility in Active Matter Systems: Fluctuation Theorem and Mutual Information, *Phys. Rev. X*, 2019, **9**, 021009.

25 L. Dabelow and R. Eichhorn, Irreversibility in active matter: General framework for active Ornstein-Uhlenbeck particles. arXiv preprint arXiv:201102976. 2020.

26 D. Mandal, K. Klymko and M. R. DeWeese, Entropy Production and Fluctuation Theorems for Active Matter, *Phys. Rev. Lett.*, 2017, **119**, 258001.

27 S. Shankar and M. C. Marchetti, Hidden entropy production and work fluctuations in an ideal active gas, *Phys. Rev. E*, 2018, **98**, 020604.

28 A. Gnoli, A. Petri, F. Dalton, G. Pontuale, G. Gradenigo and A. Sarracino, *et al.*, Brownian Ratchet in a Thermal Bath Driven by Coulomb Friction, *Phys. Rev. Lett.*, 2013, **110**, 120601.

29 A. Gnoli, A. Sarracino, A. Puglisi and A. Petri, Nonequilibrium fluctuations in a frictional granular motor: Experiments and kinetic theory, *Phys. Rev. E: Stat., Nonlinear, Soft Matter Phys.*, 2013, **87**, 052209.

30 A. Gnoli, A. Puglisi, A. Sarracino and A. Vulpiani, Nonequilibrium Brownian motion beyond the effective temperature, *PLoS One*, 2014, **9**(4), e93720.

31 S. Joubaud, D. Lohse and D. van der Meer, Fluctuation Theorems for an Asymmetric Rotor in a Granular Gas, *Phys. Rev. Lett.*, 2012, **108**, 210604.

32 K. Cheng, J. Q. Dong, W. H. Han, F. Liu and L. Huang, Infima statistics of entropy production in an underdamped Brownian motor, *Phys. Rev. E*, 2020, **102**, 062127.

33 N. Kumar, H. Soni, S. Ramaswamy and A. Sood, Flocking at a distance in active granular matter, *Nat. Commun.*, 2014, **5**(1), 1–9.

34 N. Kumar, S. Ramaswamy and A. K. Sood, Symmetry Properties of the Large-Deviation Function of the Velocity of a Self-Propelled Polar Particle, *Phys. Rev. Lett.*, 2011, **106**, 118001.

35 M. C. L. Lugo, K. C. C. Bayer, S. G. Gonzales and M. N. P. Confesor, λ-Like transition in the dynamics of ratchet gears in active bath, *Phys. Rev. E*, 2020, **102**, 052607.

36 V. Holubec and R. Marathe, Underdamped active Brownian heat engine, *Phys. Rev. E*, 2020, **102**, 060101.

37 G. Szamel, Self-propelled particle in an external potential: Existence of an effective temperature, *Phys. Rev. E: Stat., Nonlinear, Soft Matter Phys.*, 2014, **90**, 012111.

38 C. Maggi, M. Paoluzzi, L. Angelani and R. Di Leonardo, Memory-less response and violation of the fluctuationdissipation theorem in colloids suspended in an active bath, *Sci. Rep.*, 2017, **7**(1), 1–7.

39 J. O. Daldrop, B. G. Kowalik and R. R. Netz, External Potential Modifies Friction of Molecular Solutes in Water, *Phys. Rev. X*, 2017, **7**, 041065.

40 A. Sarracino, D. Villamaina, G. Gradenigo and A. Puglisi, Irreversible dynamics of a massive intruder in dense granular fluids, *EPL*, 2010, **92**(3), 34001.

41 L. Guan, L. Tian, M. Hou and Y. Han, Dynamics of a vibration-driven single disk, *Sci. Rep.*, 2021, **11**(1), 16561.